Cathode Materials

International Edition: DOI: 10.1002/anie.201501165
German Edition: DOI: 10.1002/ange.201501165

Superstructure in the Metastable Intermediate-Phase $Li_{2/3}FePO_4$ Accelerating the Lithium Battery Cathode Reaction**

*Shin-ichi Nishimura, Ryuichi Natsui, and Atsuo Yamada**

Abstract: *$LiFePO_4$ is an important cathode material for lithium-ion batteries. Regardless of the biphasic reaction between the insulating end members, Li_xFePO_4, $x \approx 0$ and $x \approx 1$, optimization of the nanostructured architecture has substantially improved the power density of positive $LiFePO_4$ electrode. The charge transport that occurs in the interphase region across the biphasic boundary is the primary stage of solid-state electrochemical reactions in which the Li concentrations and the valence state of Fe deviate significantly from the equilibrium end members. Complex interactions among Li ions and charges at the Fe sites have made understanding stability and transport properties of the intermediate domains difficult. Long-range ordering at metastable intermediate eutectic composition of $Li_{2/3}FePO_4$ has now been discovered and its superstructure determined, which reflected predominant polaron crystallization at the Fe sites followed by Li^+ redistribution to optimize the Li–Fe interactions.*

Mixed ion–electron conducting solid materials have many important functions, such as providing energy storage in batteries, mediating thermoelectric energy conversion, and serving as a catalyst of fuel-cell reactions. Reversible energy storage in solid electrode materials for batteries is a typical example of this. However, correlation science for multiple condensed mobile species in solids has not been established to date, despite a very long history of research on the rechargeable batteries and the deep penetration of this technology into our daily lives. Herein we try to achieve some general implications on how opposite charges (ions and electrons) move together in mixed conductors, using the typical electrode materials in lithium ion batteries.

The lithium ion battery (LIB) is the most advanced energy storage system currently available, but its applications have long been limited to portable electronic devices because of cost and safety issues. However, LIBs are now beginning to be applied to larger-scale applications such as electric vehicles. Ceramic mixed-ion electron-conducting oxides, which include lithium and transition metals such as $LiMO_2$ (M = Co, Ni, Mn, Li) and $LiMn_2O_4$ are used in positive electrode of the battery.[1–3] An inexpensive material based on the abundant element Fe has been considered the holy grail of materials since the first commercialization of the LIB by Sony in 1991.[4] The use of lithium iron phosphate, Li_xFePO_4 $(0 < x < 1)$, which was proposed by Padhi et al. in 1997, has attracted considerable attention because of its highly safe nature and the high natural abundance of Fe.[5] Despite its insulating nature, with $10^{-9}\,S\,cm^{-1}$, use of small particles with carbon coating has allowed the full theoretical capacity and high-power operation to be utilized.[6,7] Since 2006, commercial $LiFePO_4$-based batteries have been available for use in power tools, stationary storage, and automobiles. However, detailed reaction mechanisms that enable the high-power operation of $LiFePO_4$-based batteries are not well established and still under debate.

Phase equilibria in the Li_xFePO_4 and its related system have been extensively studied by several research groups. Dodd et al. and Delacourt et al. provided an experimental phase diagram as a function of temperature.[8,9] The $LiFePO_4$–$FePO_4$ system is immiscible at room temperature, but is slightly miscible in the vicinity of the end members, $0 < x < \alpha$ and $1-\beta < x < 1$.[10] Thus, the movement of the phase boundary dominates the electrode reaction of Li_xFePO_4 at room temperature. The system becomes miscible by 1) increasing the temperature to 500–620 K;[8,9] 2) decreasing the particle size;[11,12] 3) substitution of Fe by other transition metal;[13,14] and 4) introducing Li–Fe anti-site defects or substituting the M1 site with Fe.[12] Computational studies based on statistical thermodynamics have revealed that the electronic and lithium configurational entropy dominate the temperature-driven immiscible–miscible transition.[15–17]

A eutectic composition is known to exist at $x \approx 2/3$.[8,18] At this specific lithium composition, a metastable solid-solution is obtained by quenching from $T \approx 620$ K to room temperature. Recently, Orikasa et al. demonstrated the in situ formation of this metastable phase in a lithium half-cell under extremely non-equilibrium conditions during the electrochemical reaction even at room temperature.[19] Subsequently, Liu et al. and Zhang et al. independently elucidated the rate-induced formation of the intermediate phase in

[*] Dr. S. Nishimura, Prof. A. Yamada
Department of Chemical System Engineering
Graduate School of Engineering, The University of Tokyo
7-3-1 Hongo, Bunkyo-ku, Tokyo 113-8656 (Japan)
E-mail: yamada@chemsys.t.u-tokyo.ac.jp
R. Natsui
Department of Electronic Chemistry
Interdisciplinary Graduate School of Science and Engineering,
Tokyo Institute of Technology
4259 Nagatsuta, Midori, Yokohama 226-8502 (Japan)

[**] This work was supported by JSPS KAKENHI grant Numbers 23245042 and 19205027. The neutron diffraction data were collected under the assistance of Prof. Toru Ishigaki at Ibaraki University. The synchrotron experiments were performed under approval of the Photon Factory Program Advisory Committee (Proposal No. 2011G683, 2013G670). Preliminary experiments were performed at SPring-8 with the approval of the Japan Synchrotron Radiation Research Institute (JASRI) (Proposal No. 2011B1872 and 2013A1665).

Supporting information for this article is available on the WWW under http://dx.doi.org/10.1002/anie.201501165.

Li_xFePO_4/Li cells.[20,21] These results illustrate that the intermediate phase plays an important role in the high-power operations of batteries even at room temperature. However, the origin of the metastability at $x \approx 2/3$ has not been experimentally clarified.

Herein, we demonstrate the presence of long-range order in the metastable $Li_{2/3}FePO_4$ phase. A polaronic charge-ordered structure was determined by combining X-ray and neutron diffraction data using selected-area electron diffraction at room-temperature.

To obtain the metastable intermediate phase of $Li_{2/3}FePO_4$, we prepared the $LiFePO_4$ powder using the conventional ceramics method. Next, the $LiFePO_4$ powder was reacted with NO_2BF_4 in an acetonitrile solution at room temperature to topochemically extract all of the lithium and form the $FePO_4$. The pristine $LiFePO_4$ and $FePO_4$ were thoroughly mixed at a molar ratio of 3:2 before sealing in an evacuated quartz glass tube. Here, a use of the ratio 3:2 instead of the target 2:1 was effective to suppress the nucleation of the thermodynamically stable $Li_{x\approx1}FePO_4$. The ampoule was annealed at 623 K to form a homogeneous solid solution. Subsequently, the ampoule was dropped into cold water to obtain the metastable phase.

Figure 1a shows a high-resolution powder X-ray diffraction (HR-XRD) pattern for the metastable $Li_{2/3}FePO_4$ phase. Weak Bragg reflections observed at $d = 11.64$ and 5.82 Å, which clearly suggested the presence of longer-range periodicities. Along with the superlattice reflections, the fundamental reflections show peak splittings (for example 210_{Pnma}) that are due to a monoclinic distortion of the fundamental lattice. The selected area electron diffraction patterns in Figure 1b suggest a three-fold superstructure in the *ab* plane of the original *Pnma* lattice. No superlattice reflections are observed along the *c* direction. A monoclinic supercell with a transformation matrix of:

$$\mathbf{P} = \begin{pmatrix} 1 & 0 & 0 \\ -1 & 3 & 0 \\ 0 & 0 & 1 \end{pmatrix} \quad (1)$$

satisfies all of the observed super-reflections and peak splittings in the HR-XRD pattern. Furthermore, systematic extinction of the diffraction intensities suggested a monoclinic space group $P2_1/n$. Here we adopt a non-standard setting (unique axis *c*) to clarify the orientation relationship with the original *Pnma* structure.

Figure 2 shows the observed and calculated diffraction patterns of the final refinement results. Further crystallographic information is summarized in Table S1 and S2 in the Supporting Information. Simultaneous refinement of the neutron and X-ray diffraction patterns revealed that the metastable phase maintains the original olivine framework (Supporting Information, Figure S1). Slight differences are observed in small displacements of the atoms from their original positions, where the oxygen atoms showed larger displacements than the other atoms. Because the diffraction pattern suggests that the sample contained 6.8(2) wt% of $FePO_4$, the Li concentration in the major metastable phase was expected to approximately 0.67, which is consistent with the refined Li occupancies in the $Li_{2/3}FePO_4$ phase of 0.67(4).

According to the Vegard's law, the expected volume of the fundamental unit cell of $Li_{2/3}FePO_4$ is 282.99 $Å^3$, while the actual volume was much larger, 286.733(4) $Å^3$ (860.20(12) $Å^3$ for the superlattice). This result indicates the existence of strong repulsive interactions between the introduced Fe^{3+} and

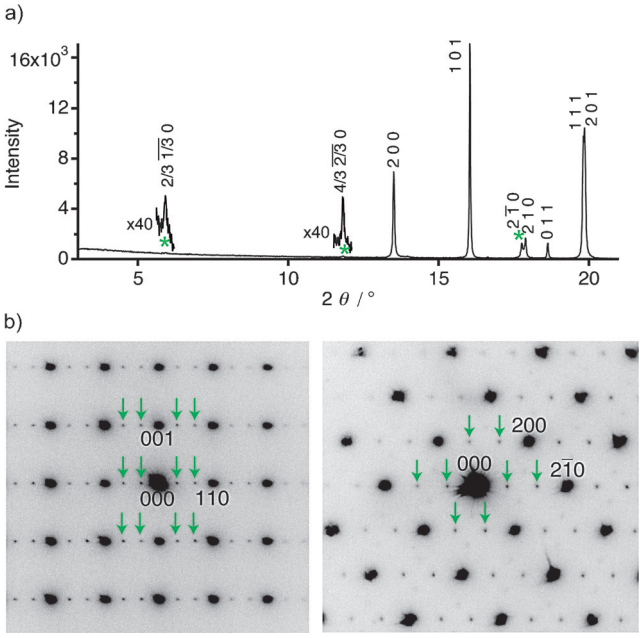

Figure 1. a) Synchrotron powder X-ray diffraction (XRD) pattern (two remarkable reflections are expanded for clarity). b) Selected-area electron diffraction patterns of metastable mixed-valence-phase $Li_{2/3}FePO_4$. Green marks indicate the positions of superstructure reflections. $[\bar{1}10]_{Pnma}$ (left) and $[001]_{Pnma}$ (right) show a clear three-fold superstructure in the *ab* plane of the original *Pnma* lattice.

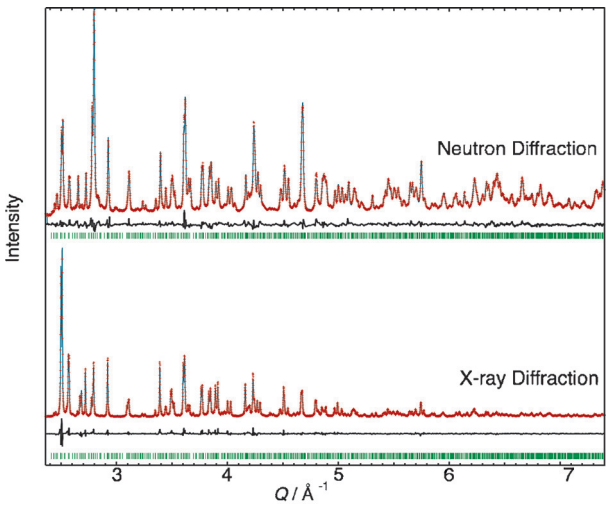

Figure 2. Rietveld refinement patterns for a) the time-of-flight neutron diffraction profile measured and b) the synchrotron X-ray diffraction profile measured for $Li_{2/3}FePO_4$ at room-temperature. The data points are plotted against the scattering vector $Q = 4\pi(\sin\theta)/\lambda$. The observed and calculated intensities are represented as red crosses and cyan lines, respectively. The Bragg positions are plotted as green tick marks, and the black curves represent the residual difference.

the Li^+, which are known to be the main driving force of phase separation in the $LiFePO_4$–$FePO_4$ systems.[15]

Some nonstoichiometric olivine compounds exhibit defect-ordered structures. For example, natural laihunite, an oxidized form of fayarite $\square_{0.4}Fe^{2+}_{0.8}Fe^{3+}_{0.8}SiO_4$, shows a three-fold superstructure, which originates from a vacancy ordering of Fe at the M1 site.[22] A similar behavior occurs when vacancies are introduced in $LiFePO_4$. Hamlet et al. reported a superstructure that resulted from the ordering of Fe(M2) vacancies, which are introduced bx oxidation of pristine $LiFePO_4$ by heating at moderate temperature in air.[23] However, these defect ordering models do not explain the superstructure observed in the present system.

Owing to the high Li mobility in the one-dimensional channel,[24] lithium ordering with an intra-channel configuration is expected. However, the refined Li occupancies are larger than 0.4 for all four of the crystallographic sites. Furthermore, all of the lithium sites had significant probability densities in difference Fourier analysis that used a structural model without lithium. These results indicate that no perfect lithium-vacancy orderings occurred with occupancies of one or null. In contrast, the valence states of Fe showed a clear long-range ordering signature. Crystallographically, the Fe sites take three individual positions, which are denoted as Fe1, Fe2, and Fe3. Only the Fe2 site has a shorter mean Fe–O bond length than the other sites by ca. 0.12 Å. The bond valence sum (BVS) that were calculated from standard parameters were 2.03 for Fe1, 2.98 for Fe2, and 1.93 for Fe3 (Supporting Information, Table S4).[25] All of the values were close to 2 or 3, which indicate that the valence states were disproportionately in the two distinct ionic valence states of Fe^{2+} and Fe^{3+}. This feature is similar to the electrostatically driven charge ordering in $Fe^{+2}Fe^{+3}OBO_3$.[26] Furthermore, ^{57}Fe Mössbauer spectroscopy supports this proposal. The spectrum contains Fe^{II} and Fe^{III} doublets, which show the typical isomer shifts and quadrupole splittings of octahedrally coordinated phosphates (Supporting Information, Figure S2 and Table S3). Consequently, the primary origin of the long-range ordering is the charge-ordering at the Fe sites. Thus, this metastable phase is written as $Li_{2/3}[Fe^{2+}_{2/3}Fe^{3+}_{1/3}]PO_4$.

Olivine-type Na_xFePO_4 system forms a stable intermediate phase $Na_{2/3}FePO_4$.[27,28] Boucher et al. recently unraveled a superstructure in the $Na_{2/3}FePO_4$, in which charge ordering at Fe coexists with Na/vacancy ordering.[28] They also provided a hypothetical superstructure of $Li_{2/3}FePO_4$ using the $Na_{2/3}FePO_4$ as a starting model by density functional calculations. We demonstrate the experimentally solved structure of $Li_{2/3}FePO_4$ for the first time, which provides advanced understandings on competitive ordering behavior of Li/vacancy versus Fe^{+3}/Fe^{2+}. The final definitive structure can be understood by predominant charge ordering of Fe ions followed by redistribution of Li ions to optimize local interaction. This has naturally led to statistical distribution of Li ions to all possible crystallographic sites with variable occupancy.

Figure 3 illustrates the charge-ordering pattern, in which charge stripes run along $[1\bar{1}0]_{Pnma}$. This pattern can be understood because of the minimizing electrostatic repulsion among the Fe^{3+} ions in the Fe sublattice. The observed superreflections in Figure 1 are not from these stripes, but rather from the static polaronic distortions (that is, electron–lattice interactions) in the charge-ordered state that induce a commensurate structural modulation along $[2\bar{1}0]_{Pnma}$.

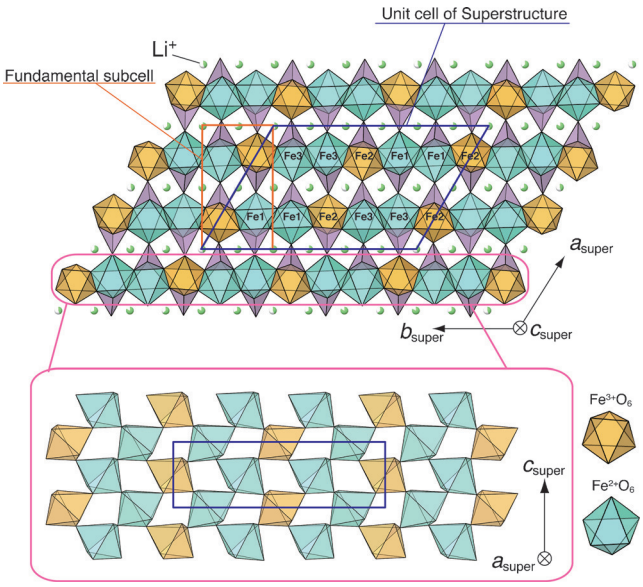

Figure 3. Illustration of the superstructure in $Li_{2/3}FePO_4$. Fe sites show a stripe-type charge ordering in the *ab* plane along [110]. Green fraction of Li spheres indicates occupancy of each Li sites.

Finally, we examined the correlation between the Li occupancies and the charge ordering. As shown in Figure 4, the Li and the Fe have different sublattices. The Li forms a one-dimensional lattice, while the Fe forms a highly distorted pseudo two-dimensional square lattice. Simultaneous satisfaction of the least-frustration configuration is not possible for both of sublattices in the olivine structure. However, each Li site has a distinct Fe^{2+}:Fe^{3+} ratio for second-

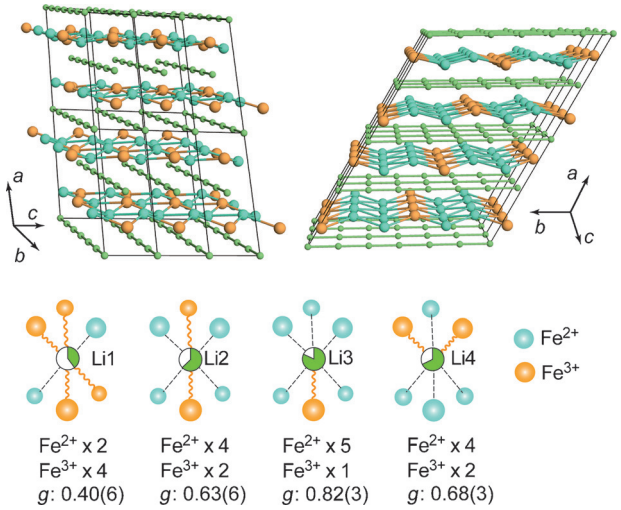

Figure 4. a) Fe and Li sublattices in the Li_xFePO_4 structure, and b) representations of the Li–Fe interaction in charge-ordered $Li_{2/3}FePO_4$. Fe and Li sublattices have different geometries and cause electrostatic frustration between Li^+ ion and Fe^{3+} ion.

nearest coordination with related occupancies. The Li site with the larger occupancy is surrounded by a larger number of Fe^{3+} and vice versa. This trend suggests that the Li–Fe interaction is present in the current charge-ordered and Li-disordered models.

In conclusion, we discovered long-range ordering in the metastable intermediate phase $Li_{2/3}[Fe^{2+}_{2/3}Fe^{3+}_{1/3}]PO_4$. The intermediate can function as a buffer to relax lattice mismatch between two end members, $Li_{x\approx0}FePO_4$ and $Li_{x\approx1}FePO_4$, to accelerate the phase boundary movement, as Orikasa et al. has pointed out. Also, this lithium-deficient and mixed-valent state is expected to induce higher ionic/electronic conductivity than the pristine $LiFePO_4$ and $FePO_4$, and possibly enhance reaction kinetics. The structural analysis revealed that the charge-ordered stripes at the Fe sites and the disordered configuration of lithium resulted from the electrostatic frustrations among the lithium and Fe^{3+} ions. The localized polarons and the disordered Li configuration suggested that the lithium is highly mobile, in contrast to the localized polarons, which have a sluggish nature. These results from multiple experiments agree and provide strong evidence for the proposed metastable superstructure and its origins. Our model also explains origin of the formation of intermediate phase at extremely non-equilibrium conditions during the $LiFePO_4$ cathode reaction. The comprehensive understanding obtained here regarding the metastable intermediate during the electrochemical reaction may have general implications for understanding mixed conducting energy storage and catalytic materials in which the localized polarons coexist with faster ionic conduction. Many of the functional materials are of this type.

Keywords: cathode materials · $LiFePO_4$ · lithium-ion batteries · olivine · solid-state structures

How to cite: *Angew. Chem. Int. Ed.* **2015**, *54*, 8939–8942
Angew. Chem. **2015**, *127*, 9067–9070

[1] K. Mizushima, P. C. Jones, P. J. Wiseman, J. B. Goodenough, *Mater. Res. Bull.* **1980**, *15*, 783–789.
[2] T. Ohzuku, Y. Makimura, *Chem. Lett.* **2001**, 642–643.
[3] M. M. Thackeray, P. J. Jhonson, L. A. de Picciotto, P. G. Bruce, J. B. Goodenough, *Mater. Res. Bull.* **1984**, *19*, 179–187.
[4] J. B. Goodenough, K.-S. Park, *J. Am. Chem. Soc.* **2013**, *135*, 1167–1176.
[5] A. K. Padhi, K. S. Nanjundaswamy, J. B. Goodenough, *J. Electrochem. Soc.* **1997**, *144*, 1188–1194.
[6] A. Yamada, S. C. Chung, K. Hinokuma, *J. Electrochem. Soc.* **2001**, *148*, A224–A229.
[7] N. Ravet, S. Besner, M. Simonear, P. Hovington, M. Armand, *The Electrochemical Society of Japan Meeting Abstracts* **1999**, 99–2, Abstract127.
[8] J. Dodd, R. Yazami, B. Fultz, *Electrochem. Solid-State Lett.* **2006**, *9*, A151–A155.
[9] C. Delacourt, P. Poizot, J. M. Tarascon, C. Masquelier, *Nat. Mater.* **2005**, *4*, 254–260.
[10] A. Yamada, H. Koizumi, S. Nishimura, N. Sonoyama, R. Kanno, M. Yonemura, T. Nakamura, Y. Kobayashi, *Nat. Mater.* **2006**, *5*, 357–360.
[11] G. Kobayashi, S. Nishimura, M.-S. Park, R. Kanno, M. Yashima, T. Ida, A. Yamada, *Adv. Funct. Mater.* **2009**, *18*, 1–9.
[12] P. Gibot, M. Casas-Cabanas, L. Laffont, S. Levasseur, P. Carlach, S. Hamelet, J.-M. Tarascon, C. Masquelier, *Nat. Mater.* **2008**, *7*, 741–747.
[13] A. Yamada, Y. Kudo, K.-Y. Liu, *J. Electrochem. Soc.* **2001**, *148*, A1153–A1158.
[14] A. Yamada, Y. Kudo, K.-Y. Liu, *J. Electrochem. Soc.* **2001**, *148*, A747–A754.
[15] F. Zhou, T. Maxisch, G. Ceder, *Phys. Rev. Lett.* **2006**, *97*, 155704.
[16] R. Malik, F. Zhou, G. Ceder, *Nat. Mater.* **2011**, *10*, 578–590.
[17] R. Malik, F. Zhou, G. Ceder, *Phys. Rev. B* **2009**, *79*, 214201.
[18] G. Chen, X. Song, T. J. Richardson, *J. Electrochem. Soc.* **2007**, *154*, A627–A632.
[19] Y. Orikasa, T. Maeda, Y. Koyama, H. Murayama, K. Fukuda, H. Tanida, H. Arai, E. Matsubara, Y. Uchimoto, Z. Ogumi, *J. Am. Chem. Soc.* **2013**, *135*, 5497–5500.
[20] H. Liu, F. C. Strobridge, O. J. Borkiewicz, K. M. Wiaderek, K. W. Chapman, P. J. Chupas, C. P. Grey, *Science* **2014**, *344*, 1252817.
[21] X. Zhang, M. van Hulzen, D. P. Singh, A. Brownrigg, J. P. Wright, N. H. van Dijk, M. Wagemaker, *Nano Lett.* **2014**, *14*, 2279–2285.
[22] B. Shen, O. Tamada, M. Kitamura, N. Morimoto, *Am. Mineral.* **1986**, *71*, 1455–1460.
[23] S. Hamelet, M. Casas-Cabanas, L. Dupont, C. Davoisne, J. M. Tarascon, C. Masquelier, *Chem. Mater.* **2011**, *23*, 32–38.
[24] S. Nishimura, G. Kobayashi, K. Ohoyama, R. Kanno, M. Yashima, A. Yamada, *Nat. Mater.* **2008**, *7*, 707–711.
[25] I. D. Brown, D. Altermatt, *Acta Crystallogr. Sect. B* **1985**, *41*, 244–247.
[26] J. P. Attfield, A. M. T. Bell, L. M. Rodriguez-Martinez, J. M. Greneche, R. J. Cernik, J. F. Clarke, D. A. Perkins, *Nature* **1998**, *396*, 655–658.
[27] P. Moreau, D. Guyomard, J. Gaubicher, F. Boucher, *Chem. Mater.* **2010**, *22*, 4126–4128.
[28] F. Boucher, J. Gaubicher, M. Cuisinier, D. Guyomard, P. Moreau, *J. Am. Chem. Soc.* **2014**, *136*, 9144–9157.

Received: February 12, 2015
Revised: April 24, 2015
Published online: June 12, 2015

